A Journal of the Gesellschaft Deutscher Chemiker

Angewandte International Edition GDCh Chemie

www.angewandte.org

Accepted Article

Title: H_2S-activable MOF Nanoparticle Photosensitizer for Effective Photodynamic Therapy against Cancer with Controllable Singlet-oxygen Release

Authors: Yu Ma, Xiangyuan Li, Aijie Li, Peng Yang, Caiyun Zhang, and Bo Tang

To be cited as: *Angew. Chem. Int. Ed.* 10.1002/anie.201708005
Angew. Chem. 10.1002/ange.201708005

Link to VoR: http://dx.doi.org/10.1002/anie.201708005
http://dx.doi.org/10.1002/ange.201708005

WILEY-VCH

10.1002/anie.201708005

WILEY-VCH

H_2S-activable MOF Nanoparticle Photosensitizer for Effective Photodynamic Therapy against Cancer with Controllable Singlet-oxygen Release

Yu Ma, Xiangyuan Li, Aijie Li, Peng Yang, Caiyun Zhang, and Bo Tang *

Abstract: Photodynamic therapy (PDT) has emerged as an important minimally invasive tumor treatment technology. The search for an effective photosensitizer to realize selective cancer treatment has become one of the major focus in recent developments of PDT technology. Controllable singlet-oxygen release based on specific cancer-associated events, as another major layer of selectivity mode, has attracted great attention in recent years. Here, for the first time, we demonstrated that a novel mixed-metal functionalized metal-organic framework nanoparticle (MOF NP) photosensitizer can be activated by a hydrogen sulfide (H_2S) signaling molecule in a specific tumor microenvironment for PDT against cancer with controllable singlet-oxygen release in living cells. The effective removal of tumors in vivo further confirmed the satisfactory treatment effect of the MOF NP photosensitizer.

Photodynamic therapy (PDT), as a new minimally invasive tumor treatment technology, has attracted great attention for its satisfactory clinical effects.[1] Compared with conventional therapeutics, such as surgery, chemotherapy and radiation therapy, PDT treatment possesses several unique advantages including noninvasiveness, negligible drug resistance, quick curative effect, repeatable administration without cumulative toxicity, no inhibition to the host immune system and low side effects.[1a,2] Specifically, PDT treatment involves three key components: a photosensitizer (PS), a light source and reactive oxygen species (ROS). Upon irradiation, the excited PS transfers energy to the surrounding oxygen in the tissue to generate ROS, which can be exploited to induce cell apoptosis and necrosis.[3] From the view point of the entire treatment process, the PS is the key factor in determining the antitumor efficacy. Porphyrin derivatives and its analogues are the main clinically used PSs currently.[4] However, due to their hydrophobic nature, insufficient tumor localization, easy accumulation, limited permeation and retention (EPR) effect and/or complex synthetic modification, etc,[5] the design and synthesis of simple and effective delivery systems with precisely controlled composition for porphyrinic molecules to the tumor sites has become an important research subject.

Metal-organic framework nanoparticles (MOF NPs), as a new type of miniature crystalline porous MOF materials constructed from metal ions/clusters and organic linkers (or bridging ligands), have been extensively studied. Combining the benefits of nanostructures and the intrinsic properties of bulk crystalline MOFs, such as the controllable composition, high porosity, large surface area, abundant in metal active sites, potential for post-synthetic modification and good biocompatibility, these materials, acted as effective nanoparticle-based delivery platforms, have shown great potential in biomedical applications.[6] Thus far, only a few examples of MOF NP PSs with molecular PSs as bridging ligands or embedded in the framework for PDT have been reported.[7] Among these systems, only one MOF NP platform investigated targeting by folate post modification.[7a] However, spatiotemporal controllable ROS release based on specific cancer-associated events, as another major layer of selectivity mode, has not been achieved in these novel MOF NP delivery systems.

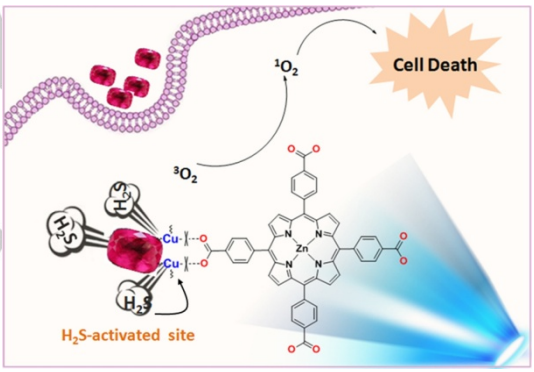

Figure 1. Simple structural fragment of MOF NP-1 and the proposed strategy for $^1O_2$ generation in cancer therapy.

In the present work, for the first time, we demonstrated that a novel mixed-metal functionalized MOF NP PS can be activated by hydrogen sulfide (H_2S) in a specific tumor microenvironment for effective treatment of colon adenocarcinoma cancer, according to the fact that the content of H_2S is significantly high in human colon adenocarcinoma cells[8]. As far as we known, this controllable singlet-oxygen ($^1O_2$) release based on H_2S-activation has not been reported thus far. On account of another fact that metalated derivatives of PSs can effectively modulate photodynamic activity,[9] we first employed zinc metalated 5,10,15,20-tetrakis(4-methoxycarbonylphenyl)porphyrin (ZnTcpp) as a photosensitive bridging ligand to construct a novel single-component MOF NP PS. Then, Cu^{2+} ions, an important H_2S-responding site in H_2S fluorescence probes,[10] were selected as metal nodes of the network. As expected, the paramagnetic Cu^{2+} ions not only completely quenched the ligand-based fluorescence of the MOF NPs but also significantly minimized the ROS production efficiency of the photosensitive ligand. When H_2S appeared, the Cu^{2+} ions were taken out from the

[*] Dr. Y. Ma,[+] X. Li,[+] A. Li, Dr. P. Yang, C. Zhang, Prof. B. Tang
College of Chemistry, Chemical Engineering and Materials Science
Collaborative Innovation Center of Functionalized Probes for Chemical Imaging in Universities of Shandong, Key Laboratory of Molecular and Nano Probes, Ministry of Education, Institute of Molecular and Nano Science, Shandong Normal University
Jinan 250014, P. R. China
E-mail: tangb@sdnu.edu.cn
[+] These authors contributed equally.

Supporting information for this article is given via a link at the end of the document.

MOF nodes, and thus, the luminophor photosensitive ligand was simultaneously obtained. In other words, this turn-on type single-component fluorescence MOF NP PS should be able to achieve effective cancer therapy with controllable photosensitive ligand release. The details of this strategy have been illustrated in Figure 1.

The new nanoscale copper-zinc mixed-metal organic-framework $\{Cu_2(ZnTcpp)\cdot H_2O\}_n$ (NP-1) was prepared via a hydrothermal microemulsion method. Based on the consideration that Cu^{2+} ions are preferable to coordinate with nitrogen atoms,[11] Zn^{2+} metalation of the porphyrin ligand within the N-containing heterocycle with $ZnCl_2$ was first carried out. Then, NP-1 was obtained by the reaction of the ligand ZnTcpp and $Cu(NO_3)_2\cdot 3H_2O$ in reverse microemulsion system under hydrothermal conditions (for details, see Supporting Information).

Our efforts to grow bulk single crystals suitable for X-ray crystallographic measurement did not succeed. Fortunately, the powder X-ray diffraction (PXRD) pattern for NP-1 is in good agreement with that of a $\{Cu_2(CuTcpp)\cdot H_2O\}_n$ MOF thin films[12] (Figure S1). In addition, the Cu/Zn ratio from energy-dispersive spectrum (EDS) illustrated that the porphyrin centers were completely occupied by Zn^{2+} ions (Figure S2). These measurements all reveal that NP-1 also exhibits two-dimensional (2D) layer networks. In this structure, each porphyrin linker, with the center site occupied by a Zn^{2+} ion is coordinated to four different $Cu_2(COO)_4$ paddlewheel units through the carboxylate groups and interconnects these binuclear paddlewheel units into 2D infinite layers. All the parallel layers are slipped with each other and further stacked into a 3D supramolecular architecture through weak interactions (e.g. hydrogen bonds and/or van der Waals interactions). This stacking mode provides the maximum PS loading compared with other MOF NPs photosensitizer so far (calcd 85.7%), which is necessary to achieve highly effective PDT of cancers once the Cu^{2+} switch is triggered.

The typical uniform plate morphology of the as-synthesized NP-1 was confirmed by transmission electron microscopy (TEM) images. As shown in Figure S3, the MOF NP plates possess an average diameter of 120 nm. Dynamic light scattering (DLS) measurements provided an average size of 105 nm for the NPs (Figure S4). This PS with suitable size showed fine aqueous dispersibility and no need for toxic organic cosolvent (Figure S3). After being immersed in the phosphate-buffered saline (PBS) and in serum proteins for 14 d at room temperature and at 50 °C, respectively, the PXRD patterns were still in good agreement with that of as-synthesized NP-1, indicating that NP-1 has sufficient stability in aqueous medium under physiological conditions (Figure S1).

Subsequently, we investigated the spectroscopic properties of NP-1. The adsorption spectrum of NP-1 displayed a Soret band at 442 nm and two Q bands at 560 nm and 600 nm (Figure 2a). The number of Q bands decreased compared to the spectrum of H_2Tcpp, which illustrates that the porphyrin centers in NP-1 have been filled with Zn^{2+} ions (Figure 2a and Figure S5). To clarify the role of H_2S in activating this nanoPS, the emission spectra were then recorded. As shown in Figure 2b,

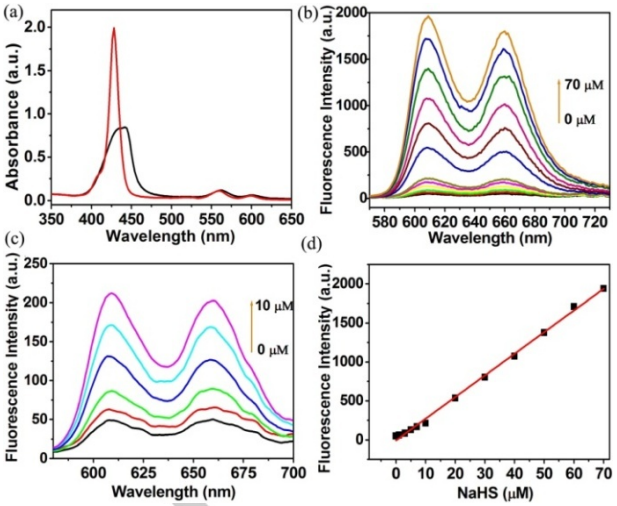

Figure 2. (a) Adsorption spectra of NP-1 (black) and ZnTcpp (red); (b) fluorescence spectra of NP-1 obtained upon titration with HS^- from 0 to 70 μM, λ_{ex} = 420 nm; (c) fluorescence spectra of NP-1 in the low-concentration region; (d) linear correlation between the fluorescence intensity and the corresponding concentration of NaHS.

upon treatment of 10 μM NP-1 with 70 μM NaHS in aqueous solution buffered at physiological pH, a considerable fluorescence enhancement was observed. To evaluate the response of the PS to the H_2S level, varying concentrations of NaHS were added to the solutions of NP-1 (10 μM) (Figure 2b and 2c). An excellent linear correlation between the fluorescence intensities and the added NaHS concentrations was observed (Figure 2d). To further establish the possibility of the efficient activation, we examined the response time of NP-1 to NaHS through reaction kinetics. As shown in Figure S6a, the fluorescence intensity reached a maximum within 1 min. All these experiments proved that NP-1 can be effectively activated by H_2S in vitro.

The experiments on selectivity were then carried out. As shown in Figure S6b, compared with the large and immediate increment of the fluorescence intensity upon the addition of 100 μM NaHS, almost no fluorescence increment was observed upon addition of abundant biologically relevant glutathione. We also examined serum protein and other reactive individual species shown in Figure S6b and S7. Similarly, these species induced no or very limited fluorescence response. All these results portended that NP-1 should be able to be selectively activated by H_2S in living cells.

The $^1O_2$ generation ability of NP-1 under irradiation in the absence and presence of H_2S was then evaluated by a $^1O_2$ probe disodium of 9,10-anthracenediyl-bis(methylene)dimalonic acid (ABMD). The ABMD molecule can react with $^1O_2$ to produce endoperoxide, which would cause a decrease in the absorption intensity of ABMD.[13] And the decreased intensity of ABMD absorption has a positive correlation with the quantity of $^1O_2$. As shown in Figure 3, the absorption intensity of ABMD quickly decreased with an extended irradiation time from 0 to 6 min in the presence of NaHS, while the variation of the absorption intensity in the absence of NaHS was very limited, almost

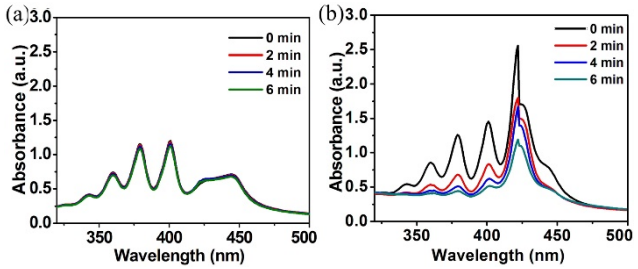

Figure 3. ABMD absorption spectra as a function of irradiation time of NP-1 before (a) and after (b) titrating with NaHS.

negligible. Therefore, we reasonably concluded that NP-1 allowed for H_2S-controllable $^1O_2$ generation.

To prove that the novel NP-1 could really be specifically activated by H_2S in living cells for cancer therapy, confocal fluorescence microscopy studies were performed on Calcein-AM and propidium (PI) stained HepG2 cells (Human hepatocellular liver carcinoma cells). As shown in Figure 4a and 4c, before being treated with NaHS, no ZnTcpp fluorescence was observed but only the fluorescence from the Calcein-AM stained cells were detected whether it is irradiated or not. These results suggested that NP-1 in living cells cannot be activated in the absence of H_2S and no cells apoptosis occurred. As a control, after being treated with NaHS but without irradiation, not only strong green fluorescence for Calcein-AM but also strong red fluorescence for ZnTcpp was observed (Figure 4b), indicating that NP-1 was activated successfully by H_2S but no apoptosis occurred. The imaging results from Figure 4b, combined with an approach based on inductively coupled plasma atomic emission spectroscopy (ICP-AES)[14] confirmed that NP-1 was indeed taken in by the HepG2 cells (for details, see the Supporting Information). However, after being treated with NaHS and irradiation simultaneously, strong red fluorescence for ZnTcpp was also observed. Compared with the control group, strong yellow fluorescence for PI was observed for the first time, but the green fluorescence for Calcein-AM disappeared, as shown in Figure 4d. This costaining imaging not only well confirmed this PS could really be specifically activated by H_2S in living cells but also confirmed the ability of H_2S-activable NP-1 for effective cancer therapy in living cells.

To further examine the PDT efficacy of NP-1 and ZnTcpp ligand, MTT assays were performed on the HepG2 cells. As shown in Figure S8a, optimal PDT efficacy was observed in the experimental groups treated with H_2S activated NP-1, while almost no cytotoxicity was observed in the dark control or blank control groups. In comparison, the ZnTcpp-treated groups with various concentrations of the ZnTcpp ligand (0-100 μM), exhibited only moderate PDT efficacy (Figure S8b). In addition, from these control groups (Figure S8-S10), we also concluded that both NP-1 and ZnTcpp themselves have good biocompatibility.

Motivated by the above results, in vivo antitumor efficacy of NP-1 was then investigated. Considering the importance of the PS in practical applications, a colon tumor model that could be treated with PDT in the clinic through an endoscope was

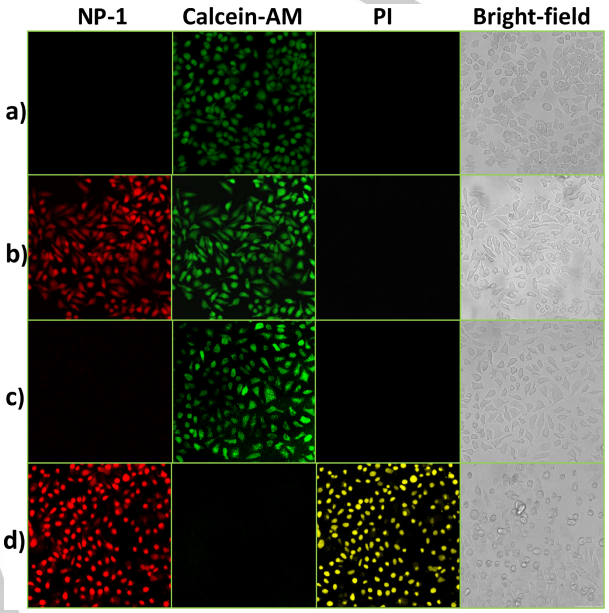

Figure 4. Confocal images of Calcein-AM and PI stained HepG2 cells with different treatments: a) 10 μM NP-1 without irradiation; b) 10 μM NP-1 and 50 μM NaHS without irradiation; c) 10 μM NP-1 with irradiation; d) 10 μM NP-1 and 50 μM NaHS with irradiation. The irradiation power was 100 mW/cm^2.

employed to estimate in vivo anticancer efficacy of NP-1. According to the fact that the content of H_2S is significantly high in human colon adenocarcinoma cells (HCT116 cells),[8] HCT116 subcutaneous xenograft nude mice were firstly prepared. After the tumor volume reached 80-100 mm^3, the mice were randomly divided into five treatment groups ($n \geq 4$, Figure 5). In the experimental group, NP-1 dispersed in PBS buffer (1.0 mg/ml) was directly injected into the tumor site of each mouse. Ten hours after the injection, the tumor region was irradiated with a 600-nm Xenon lamp at 100 mW/cm^2 for 30 min. As shown in Figure 5b, the growth of the tumor was quickly suppressed over the first two days. In contrast, the tumor growth of the control groups was not effectively suppressed (Figure 5b and S11). To further speed up the removal of the tumor and evaluate the toxicity of higher treatment doses of NP-1, the mice were treated again on the fourth day. As expected, the tumor almost disappeared within two days upon this treatment. As shown in Figure 5d, among the four tumors in the experimental group, one tumor was completely eradicated, while the sizes of the other originally larger tumors significantly decreased. Meanwhile, the body weights of all mice were continuously monitored throughout the entire treatment. As shown in Figure 5c, no obvious changes of body weight were observed. This conclusion is also in good agreement with the MTT assay on HTC116 cells in the presence of NP-1 activated by intrinsic H_2S without any stimulant (Figure 5e). Imaging fluorescence activation in HCT116 cells then further confirmed the PS could really be activated specifically by H_2S in this HCT116 subcutaneous xenograft tumor (Figure S12). In addition, the treatment efficacy

of NP-1 in terms of tumor cell death was also evaluated by H&E staining on tissue sections from the different treatment groups. The tumors treated with activated NP-1 upon irradiation

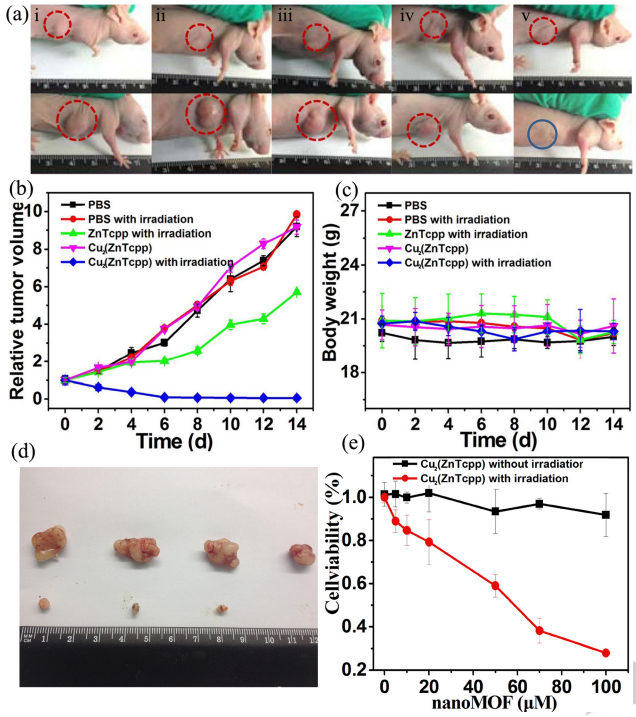

Figure 5. In vivo antitumor efficacy of NP-1 on HCT116 subcutaneous xenograft nude mice. (a) Photographs of the mice with different treatments. (b) Tumor growth inhibition curve after different treatments. (c) Mice body weight curves with relevant treatments. (d) Photo of the tumors of four parallel experimental groups after the PDT. (e) MTT assay of the HCT116 cells in the presence of different concentrations of NP-1 activated by intrinsic H_2S.

exhibited a wider range of tissue damage in tumor sections than that for only monomeric ZnTcpp, while no histopathological abnormalities were found in the tumor sections and normal tissues for other control groups (Figure S12-S16). All these results indicated that NP-1 could be effectively activated in HCT116 tumor-bearing mice by the intrinsic H_2S and provided a significant therapeutic effect safely.

To evaluate the responses for different H_2S levels in tumors, three cell lines were chosen: HCT116 cell line with the highest H_2S level among them, LoVo (human colorectal adenocarcinoma cell) cell lines with a relatively lower H_2S level, and HepG2 cell line with the lowest H_2S level. Then, these three cells subcutaneous xenograft nude mice were prepared and all their in vivo antitumor efficacy assays were performed by the same procedure as that for the HCT116 tumor-bearing nude mice. As shown in Figure S17, the tumor growth of the H_2S low expressing HepG2 and LoVo control groups treated with NP-1 under irradiation was not suppressed. Particularly, the tumor size of the HepG2 group with the lowest H_2S levels was almost the same as that of the control group, while the tumor growth of the H_2S high expressing HCT116 group treated with the same amount of NP-1 was effectively suppressed as that described above. The damaged degree of tumor tissue, evaluated by H&E staining (Figure S13 and S16), was also consistent with the above results. All these results demonstrated that under the same treatment conditions, the higher the H_2S level in tumor cells, the better the treatment effect of PDT will be obtained.

In summary, we have presented a novel MOF NP PS to achieve selective PDT for cancers. Based on the paramagnetism of the metal nodes, the MOF NPs can successfully act as a H_2S-activatable PS for controllable $^1O_2$ release. To the best of our knowledge, spatiotemporal controllable $^1O_2$ release based on specific cancer-associated events, as another major layer of selectivity mode, has not been achieved in these novel MOF NP PSs. In addition, it has been proved to be an extremely effective delivery platform with the maximum loading capability compared with the other MOF NP PS so far. Moreover, the effective removal of tumors in vivo further confirmed the satisfactory treatment effect of NP-1. With the facile modification and functionalization properties of MOFs, we anticipate these MOF NPs allow a rational design for further clinical translation. For example, this NP-1 synthesized in reverse microemulsion system combined with a PEG-modified long-circulating liposome platform, whose clinical application has been well known, will achieve longer circulation in vivo, multi-targeting and triggered release properties to cancer cells. Overall, this work not only presented a novel PS for PDT but also demonstrated the great potential of developing multifunctional MOF NP PSs for selective therapy of cancers with controllable ROS release based on other specific cancer-associated events.

Acknowledgements

This work was supported by 973 Program (2013CB933800) and National Natural Science Foundation of China (21390411, 21535004, 21675103, 21602126).

Keywords: metal organic frameworks • photodynamic therapy • controllable release • singlet-oxygen • selectivity

[1] a) D. E. J. G. J. Dolmans, D. Fukumura, R. K. Jain, *Nat. Rev. Cancer* **2003**, *3*, 380−387; b) D. K. Chatterjee, L. S. Fong, Y. Zhang, *Adv. Drug Delivery Rev.* **2008**, *60*, 1627−1637; c) L. Cheng, C. Wang, L. Feng, K. Yang, Z. Liu, *Chem. Rev.* **2014**, *114*, 10869–10939.

[2] a) G. Szakacs, J. K. Paterson, J. A. Ludwig, C. Booth-Genthe, M. M. Gottesman, *Nat. Rev. Drug Discovery* **2006**, *5*, 219–234; b) C. Bock, T. Lengauer, *Nat. Rev. Cancer* **2012**, *12*, 494–501.

[3] a) M. Ethirajan, Y. Chen, P. Joshi, R. K. Pandey, *Chem. Soc. Rev.* **2011**, *40*, 340−362; b) Y. Cheng, A. C. Samia, J. D. Meyers, I. Panagopoulos, B. Fei, C. Burda, *J. Am. Chem. Soc.* **2008**, *130*, 10643−10647; c) Z. Z. Yu, Q. Q. Sun, W. Pan, N. Li, B. Tang, *ACS Nano* **2012**, *11*, 11064–11074.

[4] a) A. Ormond, H. Freeman, *Materials* **2013**, *6*, 817-840; b) R. R. Allison, C. H. Sibata, *Photodiagn. Photodyn.* **2010**, *7*, 61−75; c) J. F. Lovell, T. W. B. Liu, J. Chen, G. Zheng, *Chem. Rev.* **2010**, *110*, 2839–2857.

[5] a) C.-K. Lim, J. Heo, S. Shin, K. Jeong, Y. H. Seo, W. D. Jang, C. R. Park, S. Y. Park, S. Kim, I. C. Kwon, *Cancer Lett.* **2013**, *334*, 176–187; b) A. Z. Wang, R. Langer, O. C. Farokhzad, *Annu. Rev. Med.* **2012**, *63*, 185−198.

[6] M. Giménez-Marqués, T. Hidalgo, C. Serre, P. Horcajada, *Coordin. Chem. Rev*. **2016**, *307*, 342–360.

[7] a) J. Park, Q. Jiang, D. W. Feng, L. Q. Mao, H.-C. Zhou, *J. Am. Chem. Soc*. **2016**, *138*, 3518−3525; b) J. Park, Q. Jiang, D. W. Feng, H.-C. Zhou, *Angew. Chem. Int. Ed*. **2016**, *55*, 1–7; c) K. D. Lu, C. B. He, W. B. Lin, *J. Am. Chem. Soc*. **2014**, *136*, 16712−16715; d) K. D. Lu, C. B. He, W. B. Lin, *J. Am. Chem. Soc*. **2015**, *137*, 7600−7603; e) K. D. Lu, C. B. He, N. N. Guo, C. Chan, K. Y. Ni, R. R. Weichselbaum, W. B. Lin, *J. Am. Chem. Soc*. **2016**, *138*, 12502−12510.

[8] C. Szabo, C. Coletta, C. Chao, K. Módis, B. Szczesny, A. Papapetropoulos, M. R. Hellmich, *PANS*, **2013**, *110*, 12474-12479.

[9] L. B. Josefsen, R. W. Boyle, *Met.-Based Drugs* **2008**, 276109.

[10] a) K. Sasakura, K. Hanaoka, N. Shibuya, Y. Mikami, Y. Kimura, T. Komatsu, T. Ueno, T. Terai, H. Kimura, T. Nagano, *J. Am. Chem. Soc*. **2011**, *133*, 18003-18005; b) Y. Ma, H. Su, X. Kuang, X. Y. Li, T. T. Zhang, B. Tang. *Anal. Chem*. **2014**, *86*, 11459-11463; c) Y.-Y. Cao, X.-F. Guo, H. Wang. *Sensors and Actuators B* **2016**, *243*, 8-13; d) X. Zhang, Q. Hu, T. F. Xia, J. Zhang, Y. Yang, Y. J. Cui, B. L. Chen, G. G. Qian. *ACS Appl Mater Interfaces* **2016**, *8*, 32259-32265.

[11] G. Aquilanti, M. Giorgetti, M. Minicucci, G. Papini, M. Pellei, M. Tegoni, A. Trasattic, C. Santini, *Dalton Trans*. **2011**, *40*, 2764−2777.

[12] G. Xu, T. Yamada, K. Otsubo, S. Sakaida, H. Kitagawa, *J. Am. Chem. Soc*. **2012**, *134*, 16524−16527.

[13] R. R. Zhang, C. L. Wu, L. L. Tong, B. Tang, Q. H. Xu, *Langmuir*, **2009**, *25*, 10153−10158.

[14] a) B. D. Chithrani, A. A. Ghazani, W. C.W. Chan, *Nano Lett*. **2006**, *6*, 662−668; b) N. Li, C. Y. Chang, W. Pan, B. Tang. *Angew. Chem. Int. Ed.* **2012**, *51*, 7426−7430.

10.1002/anie.201708005

WILEY-VCH

Entry for the Table of Contents (Please choose one layout)

COMMUNICATION

We demonstrated for the first time that a novel mixed-metal functionalized MOF NPs photosensitizer can be activated by hydrogen sulfide (H_2S) signaling molecule in specific tumor microenvironment for photodynamic therapy against cancer with controllable singlet-oxygen release.

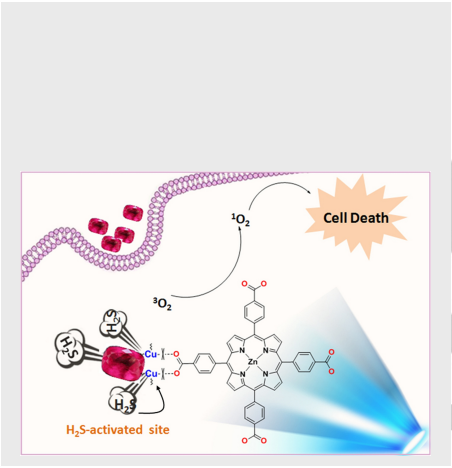

*Yu Ma, Xiangyuan Li, Aijie Li, Peng Yang, Caiyun Zhang, and Bo Tang **

Page No. – Page No.

H_2S-activable MOF Nanoparticle Photosensitizer for Effective Photodynamic Therapy against Cancer with Controllable Singlet-oxygen Release